Tessarek, Christian ; Gridenco, Oleg ; Wiesing, Martin ; Müssener, Jan ; Figge, Stephan ; Sebald, Kathrin ; Gutowski, Jürgen ; Eickhoff, Martin

Controlled Laser-Thinning of MoS2 Nanolayers and Transformation to Amorphous MoOx for 2D Monolayer Fabrication

Journal Article as: peer-reviewed accepted version (Postprint)

DOI of this document*(secondary publication): https://doi.org/10.26092/elib/3718

Publication date of this document: 21/02/2025

* for better findability or for reliable citation

Recommended Citation (primary publication/Version of Record) incl. DOI:

Controlled Laser-Thinning of MoS2 Nanolayers and Transformation to Amorphous MoOx for 2D Monolayer Fabrication. Christian Tessarek, Oleg Gridenco, Martin Wiesing, Jan Müssener, Stephan Figge, Kathrin Sebald, Jürgen Gutowski, and Martin Eickhoff ACS Applied Nano Materials 2020 3 (8), 7490-7498
DOI: 10.1021/acsanm.0c01104

Controlled Laser-Thinning of MoS_2 Nanolayers and Transformation to Amorphous MoO_x for 2D Monolayer Fabrication

Christian Tessarek,*,† Oleg Gridenco,† Martin Wiesing,‡ Jan Müssener,† Stephan Figge,† Kathrin Sebald,† Jürgen Gutowski,† and Martin Eickhoff†

†*Institute of Solid State Physics, University of Bremen, Otto-Hahn-Allee 1, 28359 Bremen, Germany*

‡*Fraunhofer Institute for Manufacturing Technology and Advanced Materials IFAM, Wiener Straße 12, 28359 Bremen, Germany*

E-mail: tessarek@ifp.uni-bremen.de

Abstract

Laser-thinning of 2D materials such as MoS_2 is a promising approach for a local reduction of the number of multilayers down to a monolayer. For a precise control of the thinning process real-time monitoring is required. In this work, short wavelength lasers emitting at 325 nm or 406 nm, respectively, are used for laser-thinning and simultaneous Raman or photoluminescence spectroscopy of MoS_2. The time-evolution of the Raman and photoluminescence bands during the process show a layer-by-layer thinning of MoS_2 and a transformation into amorphous MoO_x in an oxygen containing atmosphere. In addition to the E^1_{2g} and A_{1g} Raman modes, the E_{1g}, B^1_{2g} and second order modes are analyzed using the 325 nm laser for excitation to achieve a more accurate determination of the number of layers. As a promising alternative, photoluminescence spectroscopy

is used to monitor the thinning progress by analysis of the emission energy and intensity of the direct as well as the indirect band gap transition. Atomic force microscopy measurements show an increased total height of the laser-treated region after thinning of MoS_2 due to the presence of transformed MoO_x. Local micropatterning of a bilayer is also demonstrated by laser-thinning down to a monolayer at selected positions. The results show a new monitoring approach for controlled fabrication of 2D monolayers.

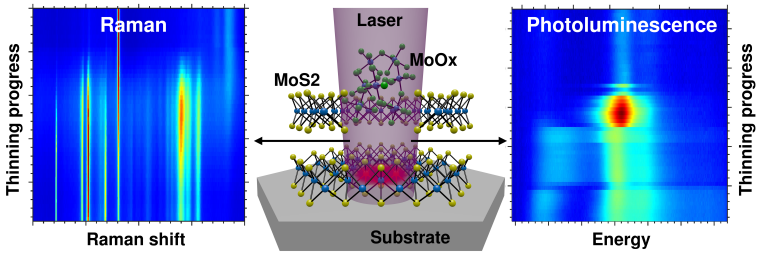

Keywords: MoS_2, laser-thinning, monitoring, UV Raman spectroscopy, photoluminescence spectroscopy, atomic force microscopy

Introduction

Two-dimensional (2D) semiconductors of the transition metal dichalcogenide (TMDC) material family such as monolayers of MoS_2, WS_2 and exfoliated WSe_2 are characterized by their direct band gap, in contrast to the indirect band gap observed for multilayers.[1–5] Thin layers of TMDCs can be produced by chemical vapor deposition,[6] molecular beam epitaxy[7] and by chemical or mechanical exfoliation of bulk crystals.[8,9] Besides the generation of monolayers each method suffers from deposition of bi- and multilayer TMDCs at the same time.[6] For electronic and opto-electronic applications such as field effect transistors, photodetectors, photovoltaic and light emitting devices[10,11] the presence of monolayers instead of a mix of randomly distributed mono- to multilayers is required. To obtain large-area monolayers it is necessary to remove additional layers. Furthermore, it is of interest to micro- and nanopattern multilayer flakes into well-defined sections with reduced layer thickness to obtain layers with desired optical and electronic properties.[12]

Laser-thinning is a promising technique to produce MoS_2 monolayers from multilay-

ers,[13–20] and Raman spectroscopy is a powerful tool to determine the number of layers.[21] Up to now, only the frequency difference between the Raman modes E^1_{2g} at $\sim$386 cm^{-1} and A_{1g} at $\sim$408 cm^{-1} is used to characterize monolayers during or after thinning.[13–16] However, for laser-thinned monolayers the frequency difference of these Raman modes can be slightly larger than that of pristine monolayers.[13–15] Thus, it is difficult to distinguish between pristine monolayers, bilayers and laser-thinned monolayers. Photoluminescence (PL) spectroscopy has so far not been used to determine the number of layers during laser-thinning. The PL intensity and wavelength of the A exciton transition strongly depends on trion and exciton densities in the layer and can also be enhanced in folded multilayers.[22] Therefore, considering only the A exciton/trion PL intensity is not sufficient to characterize monolayers. For a better control of a homogeneous monolayer generation, a more detailed monitoring of the thinning process is required.

Concerning MoS_2, additional Raman modes with comparable intensities as the E^1_{2g} and the A_{1g} modes appear if a UV laser operating at a wavelength of 325 nm is used for excitation.[23] These additional modes are E_{1g} at 288 cm^{-1}, B^1_{2g} at 470 cm^{-1} and second order Raman modes between 700-850 cm^{-1} which are usually not observed for excitation in the visible or near-infrared spectral range.[23,24] The E_{1g} mode is forbidden in backscattering configuration, but its spectral appearance was reported to be related to the breakdown of selection rules induced by resonant excitation of the mode.[23] The B^1_{2g} mode is normally inactive due to an unchanged polarizability of out of plane Mo and S vibrations, however, its activation is due to a modified crystalline point-group symmetry induced by lattice structure rearrangement close to the surface of the crystal from 325 nm excitation.[23] The Raman enhancement of the second order modes was found to originate from the occurance of an electron-two-phonon triple resonance via the deformation potential and Fröhlich interaction.[24] The intensities of the additional modes are very sensitive to the number of layers.[23,25] Therefore, tracking these additional modes during laser-thinning can enhance the precision in determining the number of layers. A more precise estimation of the layer thickness using PL is also possible

considering both the direct and the indirect band gap transitions in the visible and near infrared spectral range.[4]

In this work a method for a detailed study of laser-thinning of MoS_2 layers is proposed. First, mono- to multilayers are identified and mapped by Raman and PL spectroscopy using excitation at 325 nm and 406 nm, respectively. The peak intensities and spectral positions for different layer thicknesses are determined. The 325 nm (406 nm) laser is used for both thinning and Raman (PL) spectroscopy at the same time as it is schematically depicted in Fig. 1. The transition from trilayer via bi- and monolayer MoS_2 to completely transformed MoO_x can be observed by multiple characteristics in the Raman and PL spectra. Oxidation of MoS_2 is additionally confirmed by X-ray photoelectron spectroscopy (XPS). Atomic force microscopy (AFM) analysis shows an increased total height of the laser-treated area resulting from the transformation of MoS_2 into amorphous MoO_x that occurs simultaneously with the reduction of the number of MoS_2 layers. Employing this mechanism writing of submicron single monolayer spots in bilayer flakes is demonstrated. The results shown here present a precise method for the controlled fabrication of monolayers from 2D multilayer materials.

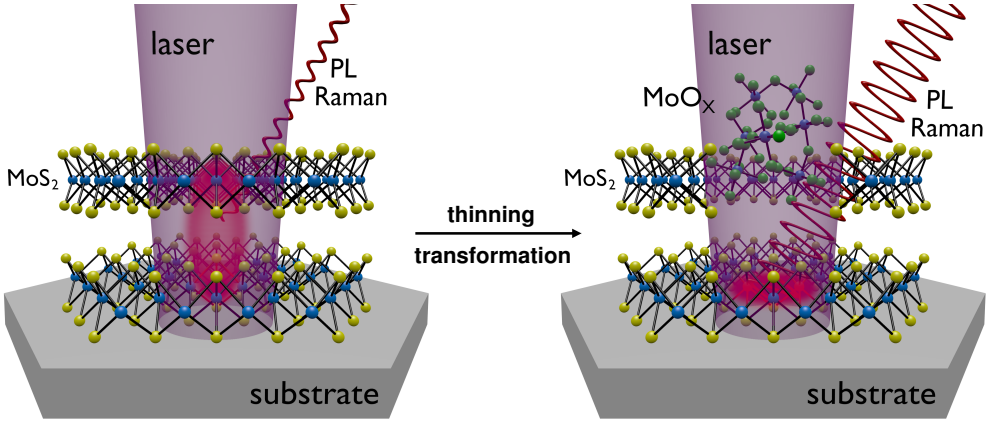

Figure 1: The schematic illustrates the situation before (left) and after (right) thinning from bi- to monolayer and transformation of the irradiated section of the upper MoS_2 layer into amorphous MoO_x. Simultaneously, laser excitation of MoS_2 leads to PL emission and Raman scattering, both visualized by the red cloud inside MoS_2 and by the red sine wave leaving the layer. Thinning-induced changes of the origin, intensity and spectral position of the Raman and PL emission are indicated by a displacement of the red cloud and an increased amplitude of the sine wave. These changes are monitored to control the thinning process.

Results and discussion

Identification of Mono- and Multilayer MoS_2. The identification of mono- and multilayers was performed by UV Raman and PL spectroscopy and mapping. Fig. 2(a) shows Raman spectra of MoS_2 flakes with different layer numbers. The frequency difference Δ between the Raman modes E^1_{2g} at $\sim$386 cm^{-1} and A_{1g} at $\sim$405 cm^{-1} increases with the number of layers and is 18.9 cm^{-1} and 21.6 cm^{-1} for a mono- and bilayer, respectively, and approaching 25 cm^{-1} for a multilayer. The Δ values are in agreement with investigations on single and multilayer MoS_2 using laser excitation in the visible range.[21] Beside the E^1_{2g} and A_{1g} Raman modes, other MoS_2-related modes such as E_{1g} at 288 cm^{-1}, B^1_{2g} at 472 cm^{-1} and the second order modes in a range between 700-850 cm^{-1} appear for excitation at 325 nm.[23] The intensity of the E_{1g} mode is weak for mono- and multilayers and exhibits a maximum for bilayers as visible in Fig. 2(b). The B^1_{2g} mode is also sensitive to the number of layers and shows its maximum intensity for trilayers (cf. Fig. 2(b)). The highest intensity of the second order modes is found for mono- and bilayers and decreases for increasing number of layers. The intensities of these additional modes are therefore suitable to differentiate between tri-, bi-, and monolayers. Finally, the Si Raman mode at 521 cm^{-1} decreases with increasing layer number due to enhanced absorption of the excitation laser in the MoS_2 layers.

PL spectra of mono-, bi-, tri-, tetra- and multilayers are shown in Fig. 2(c). The emission of the A and B exciton transition at the K and K' points of the Brillouin zone are visible at 1.81 eV and 1.97 eV, respectivly. For a monolayer, the intensity of the A exciton emission is enhanced due to the transition from an indirect to a direct band gap.[4] A comparison of the PL spectra from the bi- and monolayer shows a redshift of 0.02 eV of the A exciton-related emission, although a blueshift is expected for a decreasing the number of layers.[4] This redshift can be explained by the occurrence of charged excitons, also termed as trions, which have a lower energy than neutral excitons.[26–28] The indirect band gap transition for multilayers at 1.33 eV has a full width at half maximum (FWHM) of 0.13 eV. For decreasing layer number, it shows a blueshift which may be explained by an upshift of the conduction

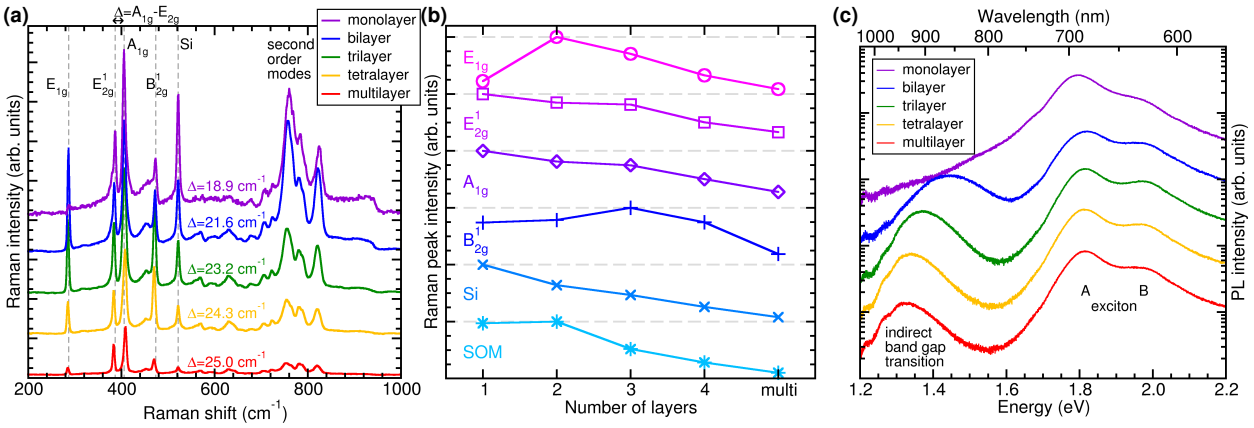

Figure 2: Raman (a) and PL (c) spectra for identification of MoS_2 mono- to multilayers excited with 325 nm and 406 nm lasers, respectively. Δ is the frequency difference between the modes E^1_{2g} and A_{1g}. (b) shows the evolution of Raman peak intensity of all modes from graph (a) with the number of layers. The Raman and PL spectra in (a) and (c) are vertically shifted for clarity. The Raman intensities in (b) are normalized with respect to the intensity maximum of each mode and vertically shifted for clarity.

band between Γ and K point and a downshift of the valance band around the Γ point, eventually enlarging the indirect band gap to 1.45 eV for the bilayer case. The energy shift with respect to the number of layers is in agreement with band structure calculations.[29] The increased FWHM up to 0.19 eV for a bilayer can be explained by a smaller curvature of the valence band around the Γ point.[30] In the case of a monolayer, the indirect band gap transition disappears.

Raman and PL spatial mapping was performed on the MoS_2 flake shown in the optical image in Fig. 3. The flake consists of mono-, bi-, tri- and multilayers, confirmed by Raman and PL measurements. The intensity distributions of selected Raman modes and the PL emission bands are shown in the left and right column of Fig. 3, respectively. Intensity maps of Raman modes and PL emission bands with similar or opposite intensity distribution are compared side by side in the lower part of the figure. The E^1_{2g} mode at 386 cm^{-1} and the emission related to the A exciton around 1.85 eV (670 nm) show the highest intensity in the monolayer regions while the intensity of the E_{1g} mode at 288 cm^{-1} and the indirect band gap transition at 1.45 eV (850 nm) are maximized in bilayer sections. For a trilayer, the B^1_{2g} mode at 472 cm^{-1} and the PL band at 1.38 eV (900 nm) show the highest intensity. The intensity

of the Si-related Raman mode at 521 cm^{-1} increases with decreasing number of layers and is maximized at regions without MoS_2. In contrast, the indirect band gap transition at 1.31 eV (950 nm) is maximized at multilayer and bulk areas and decreases with smaller number of layers.

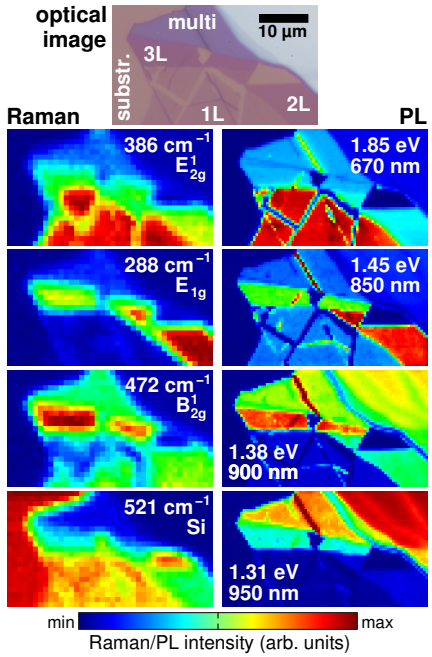

Figure 3: The figure in the top row shows an optical image of the investigated flake including monolayers (1L), bilayers (2L), trilayers (3L), multilayers (multi) and bulk MoS_2 (grey region in the upper right corner). The left and right column present the Raman and PL mapping of the area in the optical image at selcted energies. The Raman maps show the intensity distribution of E^1_{2g} (386 cm^{-1}), E_{1g} (288 cm^{-1}), B^1_{2g} (472 cm^{-1}) and the Si mode (521 cm^{-1}). The PL maps display the distribution of intensity at 1.85 eV (670 nm), 1.45 eV (850 nm), 1.38 eV (900 nm) and 1.31 eV (950 nm).

Monitoring Laser-Thinning by UV Raman Spectroscopy. Laser-thinning and simultaneous monitoring by Raman spectroscopy of an MoS_2 trilayer is performed using the 325 nm laser. Fig. 4(a) presents an intensity plot obtained from 50 Raman measurements showing the evolution of Raman modes during the thinning process. The exposure time for each spectrum/measurement was 10 s.

In Fig. 4(b) four selected Raman spectra (measurement 1, 16, 27 and 38) are presented. Spectrum no. 1 shows typical features for a trilayer such as similar maximum intensity for

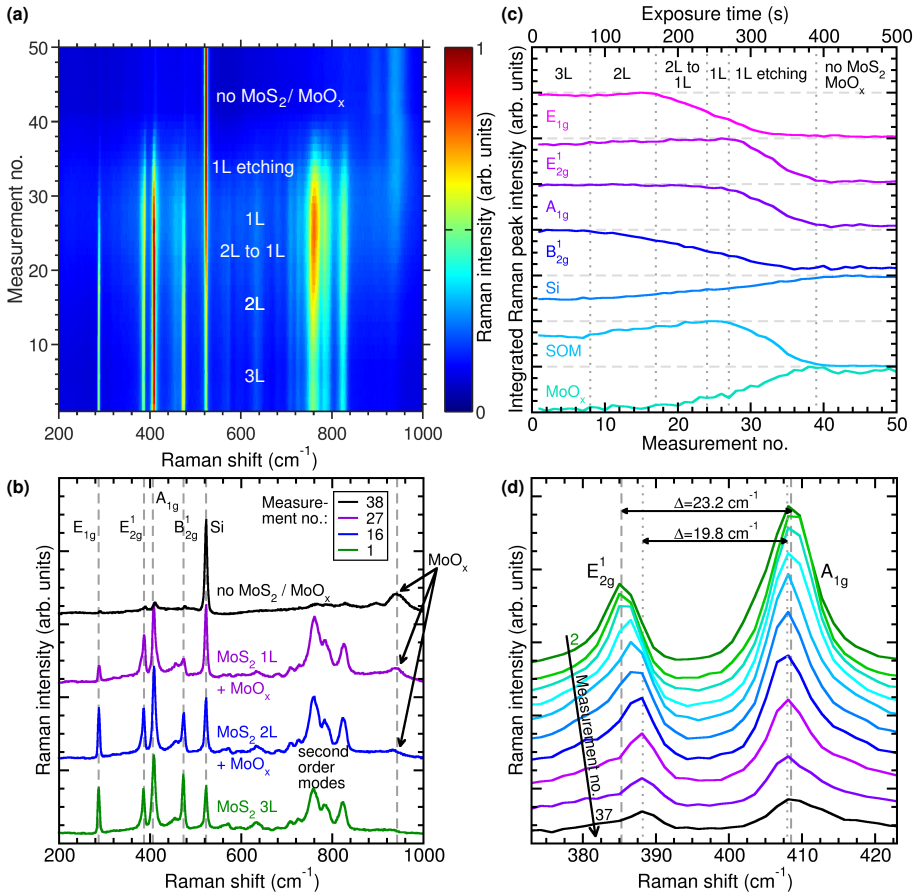

Figure 4: (a) shows an intensity plot as obtained from 50 Raman measurements recorded during laser-thinning with 325 nm laser. Selected Raman spectra from measurements 1, 27 and 38 corresponding to trilayer, monolayer and no MoS_2 / MoO_x, respectively, are displayed in (b). The evolution of the intensity of the Raman modes during laser-thinning is summarized in (c). The abbreviation SOM is used for second order modes. The Raman intensities in (c) are normalized with respect to the individual mode's maxima, respectively, and vertically shifted for clarity. (d) shows a detailed view of the thinning induced change of the frequency difference Δ of the Raman modes E^1_{2g} and A_{1g} from $23.2\,cm^{-1}$ to $19.8\,cm^{-1}$. The spectra in (b) and (d) are vertically shifted for clarity.

all MoS_2-related modes (see also Fig. 2(a)). In comparison with spectrum no. 1, the E_{1g} mode shows a slight intensity increase in spectrum no. 16 whereas the B^1_{2g} mode exhibits a certain weakening. After 27 measurements, the number of layers is reduced to one as indicated by the decrease of intensities of the E_{1g} and B^1_{2g} modes while the intensity of the second order modes has increased. MoS_2 is completely thinned after 38 measurements, as evidenced by the almost vanished MoS_2-related Raman modes. The residual E^1_{2g} and A_{1g} Raman modes result from the surrounding region, which was not thinned and is still weakly exposed due to the Gaussian laser beam profile. Two Raman modes remain in the spectrum: the Si-related mode at $521\,cm^{-1}$ and a mode at $950\,cm^{-1}$ which is not present at the beginning of the measurement series and appears after measurement no. 20. This mode is assigned to amorphous molybdenum oxide (MoO_x).[31] The appearance of the MoO_x mode during the thinning process indicates a laser-induced transformation of MoS_2 into MoO_x by oxidation with ambient O_2.[32] XPS measurements were performed to confirm the oxidation of MoS_2 by laser-thinning. Due to the $\sim$50 µm spot size of the XPS setup, a $\sim 40\times40\,\mu m^2$ area from an MoS_2 multilayer flake was laser-thinned with the 406 nm laser (see Fig. S2 in the supporting information). XPS spectra were recorded at pristine and laser-thinned MoS_2 and are shown in Fig. S3 in the supporting information. The presence of additional peaks $Mo^{6+}\,3d_{3/2}$ at 236.0 eV and $Mo^{6+}\,3d_{5/2}$ at 232.8 eV in the XPS spectrum from laser-thinned MoS_2 is attributed to oxidation of MoS_2, in agreement with literature.[14,32]

Fig. 4(c) shows the intensity evolution of each Raman mode. The transition from tri- to bilayer after measurement no. 8 is identified by an increase of the intensities of the Si-related mode and the second order modes and by an intensity decrease of the B^1_{2g} mode. The decrease of the E_{1g} mode after recording of 17 spectra indicates the transition from bi- to monolayer. A monolayer is achieved after 25 measurements when the intensity of the second order modes reaches its maximum. After 28 measurements thinning of the monolayer is evidenced by the decrease of the E^1_{2g}, A_{1g} and second order modes. All MoS_2-related modes reached their intensity minimum after 39 measurements while the Si- and MoO_x-related

modes remain almost unchanged. The results show the importance of the intensity analysis of the additional modes E_{1g}, B^1_{2g} and second order modes, which appear for 325 nm excitation only, for the unambiguous determination of number of layers. Such an analysis would not be possible with an excitation laser in the visible range where these additional modes can not be observed.[23]

In Fig. 4(d) the evolution of the E^1_{2g} and A_{1g} modes is depicted. During laser-thinning a decrease of the frequency difference Δ from 23.2 cm^{-1} to 19.8 cm^{-1} is observed. This value for Δ deviates from that obtained for pristine exfoliated MoS_2 as shown in Fig. 2(a) of 18.9 cm^{-1}. This is in agreement with other reports.[13–15] It is expected that the transformed MoO_x layer on the MoS_2 monolayer changes the dielectric screening thereby influencing the spectral position of the Raman modes.[33] Consequently, a value of $\Delta < 19\,cm^{-1}$ cannot be achieved.

In a similar laser-thinning study no MoO_x related modes were observed in the Raman spectrum using a 532 nm laser for excitation, although Mo-O bonds were found in XPS measurements.[32] Here, Raman spectra of laser-thinned MoS_2 were recorded under 325 nm and 442 nm excitation, respectively. A comparison of these spectra is shown in Fig. S4 of the supporting information. The broad MoO_x-related Raman mode at 950 cm^{-1} is visible with 325 nm but not observed with 442 nm excitation. This effect can be explained by resonant and non-resonant Raman scattering conditions for 325 nm and 442 nm excitation, respectively. The energy of 3.82 eV for the 325 nm laser is close and above the band gap of 3.59 eV of amorphous MoO_x.[34] A further effect is the Raman scattering cross-section, which is proportional to ν^4 (ν: frequency of light), so that Raman modes from the thin and amorphous MoO_x layer can rather be observed at shorter excitation wavelengths.

Monitoring Laser-Thinning by PL Spectroscopy. Alternatively to monitoring by Raman spectroscopy, laser-thinning of a trilayer MoS_2 was also carried out with the 406 nm laser while simultaneously recording PL spectra. Fig. 5(a) shows a color coded 2D plot of 55 PL measurements in a spectral range from 500 nm to 1050 nm. The exposure time of each

spectrum/measurement was 100 s in total.[35] In Fig. 5(b) selected PL spectra after 5, 15, 30 and 45 measurements corresponding to tri-, bi-, mono- and no MoS_2 layer, respectively, are shown. The MoS_2-related spectra are comparable to the ones shown in Fig. 2(c).

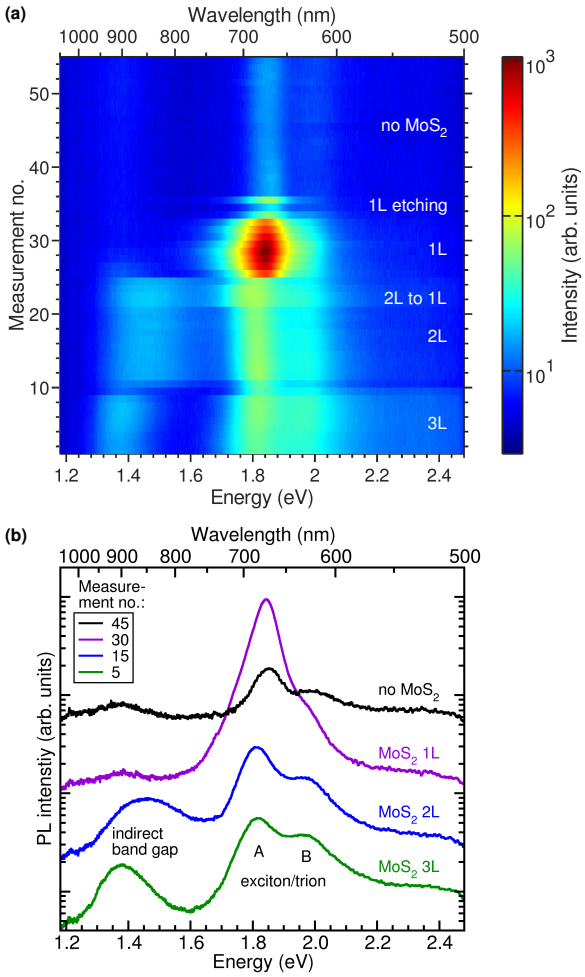

Figure 5: (a) 55 PL spectra recorded during laser-thinning of trilayer MoS_2 with a 406 nm laser. (b) PL spectra from measurements 5, 15, 30, and 45 from (a). Spectra are vertically shifted for clarity.

During the first 8 measurements, the PL remains stable with an A and B exciton-related emission at 1.82 eV and 1.95 eV, respectively. The related ratio A/B of the integrated intensity is 1.24. The indirect band gap transition is located at 1.38 eV with a FWHM of 0.14 eV, indicating the presence of a trilayer. The transition from a tri- to a bilayer is indicated by an overall decrease of PL intensity as seen for measurements no. 9 and 10 in Fig. 5(a). The reduced PL intensity is assigned to interlayer excitons, which are still partially located in

the uppermost layer and recombine non-radiatively at defects created in the laser-thinned region. The range of measurements 11 to 20 corresponds to a bilayer and shows a similar intensity as for a trilayer. No spectral shift occured for the A and B exciton, however, the ratio A/B increased to 1.49 mainly due to a slight intensity decrease of the B exciton which points to a higher defect density[36] in the bilayer caused by laser irradiation.[37] The indirect band gap emission blueshifts by 0.08 eV to 1.46 eV having a FWHM of 0.26 eV. The spectral position and the enhanced FWHM of the indirect transition is in agreement with Fig. 2(c) and indicates that the layer is thinned down from a tri- to a bilayer.

After 21 measurements the A exciton-related emission slightly redshifts to 1.81 eV, its FWHM increases from 0.12 eV to 0.15 eV, and the intensity is enhanced by a factor of 1.6. The redshift and the broadening are due to a change from exciton to trion-dominated emission[26,28] which indicates surface modifications attributed to O_2 removal. It was reported that O_2 at defect sites has a strong influence on the optical properties such as exciton- and trion-related emission for O_2 and non-O_2 containing environment, respectively.[28,38] These spectral changes after 21 measurements indicate the beginning of the transition from bi- to monolayer which is completed after 25 measurements and is indicated by a strong increase of the A exciton emission and the disappearance of the indirect band gap transition. The blueshift of the A exciton-related emission from 1.81 eV to 1.84 eV indicates a change from a trion- to an exciton-related emission.[39] This change is attributed to the high electron affinity of O_2, which adsorbs at laser-induced sulfur defect sites in the MoS_2 monolayer and reduces the n-type carrier concentration due to a charge transfer from MoS_2 to O_2.[28,38,39] After 32 measurements, a strong drop in intensity indicates further thinning of the monolayer. The total thinning of MoS_2 and the transformation of MoS_2 into MoO_x, is completed after 34 measurements. There is still a weak PL signal at 1.85 eV which stems from the surrounding residual MoS_2 layer, which is not (completely) thinned and excited by the laser due to the Gaussian spot profile.

PL spectroscopy during laser-thinning shows pronounced changes of the peak energies of

the emission bands as well as of their intensities. Thus, PL monitoring provides an easier analysis and well-defined results compared to Raman monitoring.

The increased PL intensity for a laser-thinned monolayer is clearly visible in an optical microscope. A video was recorded during laser-thinning of an MoS_2 trilayer (see Supporting Information). The 406 nm laser is exciting the center of the triangular shaped MoS_2 flake. The laser spot is not visible in the video due to a 450 nm long-pass filter placed in front of the camera. The video shows a hole evolving during exposure and red emission after thinning down to a monolayer. The red emission disappears after complete transformation of MoS_2 into MoO_x.

It is interesting to note that the tri-, bi- and monolayers exist approximately for the same number of 10-15 Raman or PL measurements during laser-thinning (see Figs. 4a and 5a). This is in contrast to other thinning experiments on 2D materials with higher laser power and lower laser energy showing a fast thinning rate for upper layers and a slow rate for the remaining monolayer.[13,40] The different thinning rates were explained by low thermal conductivity of upper MoS_2 layers and increased thermal conductivity of the monolayer, which is in direct contact with the substrate acting as a heat sink.[13] In contrast to those reports, a lower laser power (at higher laser energies) was used in this study to guarantee a slow layer-by-layer oxidation of MoS_2 at lower temperatures so that thermal conductivity plays a minor role in the thinning process.

AFM Measurements of Laser-Thinned and Transformed MoS_2. AFM measurements were carried out on an MoS_2 bilayer, which was exposed with a 406 nm laser until a complete thinning of MoS_2 and its transformation into amorphous MoO_x occurred. The surface topography of the laser treated region is shown in Fig. 6(a). Due to the presence of amorphous MoO_x, which is formed during thinning of MoS_2 by oxidation, an inner region with an increased height by about 4 nm (see height profile linescan in Fig. 6(b)) has formed, being surrounded by three nanoparticles of 6 nm height, two of them visible in the linescan. Nanoparticles decorating the laser-thinned area have also been observed in

other laser-thinning studies[15,19,32] and are formed by redeposition of amorphous or oxidized MoS_2.[32] The unexpected increased height of the laser exposed area is related to direct oxidation of MoS_2 into amorphous MoO_x and reduced redeposition of the transformed material into nanoparticles due to lower laser power used here in comparison to other studies.[15,19,32] MoS_2 and MoO_3 have similar densities, however, the density of an amorphous phase is lower compared to its crystalline counterpart[41] and, thus, a larger volume is required by the amorphous MoO_x leading to an increased height of the exposed layer. The results show that the laser treatment in ambient atmosphere is a combination of thinning of the MoS_2 layer and the formation of an amorphous MoO_x layer. As a consequence, an apparent increase of the film thickness due to MoO_x formation is observed by AFM, while Raman and PL analysis reveal the simultaneous decrease of the number of layers of MoS_2.

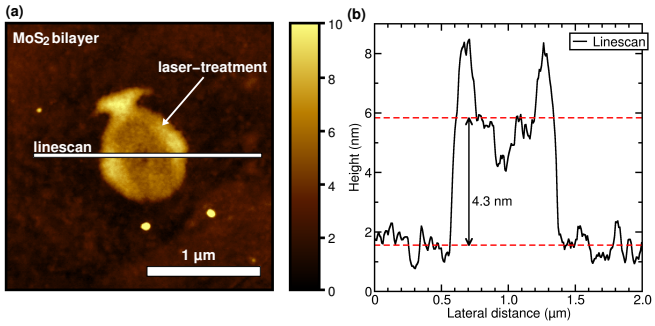

Figure 6: AFM topographical image (a) of a laser-treated MoS_2 bilayer transformed into MoO_x and the corresponding linescan (b) along the treated region.

Patterning of MoS_2 Bilayers by Laser-Thinning. Patterning of an MoS_2 layer by local laser-thinning is presented in Fig. 7. An optical image of the exfoliated MoS_2 bilayer before laser-thinning is shown in Fig. 7(a). The inset shows a homogeneous PL intensity distribution along the untreated flake. The optical image in Fig. 7(b) shows the flake after laser-thinning at five randomly selected positions which are marked by arrows. The positions A-D are thinned down to a monolayer while monitoring the A exciton-related PL emission. Thinning was stopped after enhancement of the A exciton emission intensity by a factor of 5 (see Fig. S1 in supporting information). The MoS_2 bilayer at position E was completely transformed into MoO_x, i.e. position E was exposed until the PL intensity increased and

finally decreased by a factor of 0.6, compared to the initial PL intensity. Table 1 summarizes the exposure times obtained from Fig. S1 from the supporting information. The PL intensity map around the emission band of the A exciton in Fig. 7(c) shows an enhanced (no) PL intensity at positions A-D (E). The PL map in (d) recorded around the indirect band gap emission band shows reduced PL intensity at all positions A-E. The PL maps in (c) and (d) show the successful local thinning of a bilayer down to a monolayer for positions A-D and a complete transformation at position E.

Table 1: Overview of exposure times for MoS_2 bilayer positions A-E.

Position	exposure time [s]	end state
A	1197	monolayer
B	1710	monolayer
C	1252	monolayer
D	1153	monolayer
E	1200	no MoS_2

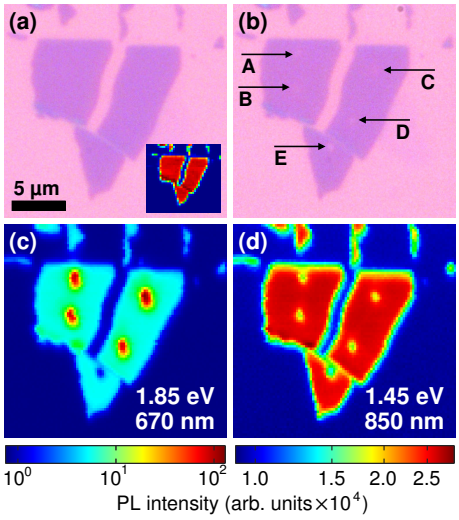

Figure 7: Optical images of the MoS_2 bilayer before (a) and after (b) local laser-thinning. The inset in (a) shows the PL map of the bilayer flake before thinning. The arrows in (b) indicate the positions A-E of the laser during thinning. Positions A-D were thinned down to a monolayer, MoS_2 at position E was completely transformed. PL intensity mapping at energies 1.85 and 1.45 eV are shown in (c) and (d), respectively.

Conclusion

Identification of MoS_2 multi- to monolayers using UV Raman and PL spectroscopy was performed with 325 nm and 406 nm laser excitation, respectively. The intensity of the ordinary and additional Raman modes, which appear for 325 nm excitation, sensitivly depend on the number of layers. Laser-thinning of MoS_2 layers was performed either with a 325 nm or 406 nm laser with simultaneous Raman or PL monitoring, respectively. During laser-thinning, the intensity change of the Raman modes is used to determine the number of layers and to monitor the transition from a trilayer down to a monolayer and further to a complete transformation of MoS_2 into amorphous MoO_x as confirmed by XPS analysis. Such a detailed determination of number of layers by analyzing the intensity of Raman modes is not possible with excitation lasers in the visible range where these additional modes are not observed. Alternatively, thinning can also be monitored by recording and analyzing intensities and energy posititions of the direct and indirect band gap transition in the PL spectra. Applying Raman or PL monitoring, a precise layer-by-layer thinning of the MoS_2 layer can be achieved. Compared to Raman spectroscopy the changes in PL during laser-thinning are even more pronounced yielding a clear and precise analysis of the number of layers. AFM measurements on a laser-thinned MoS_2 bilayer show an increased height of the treated region supporting the fact of oxidation of MoS_2 to MoO_x. Microscopic details of the transformation process such as the formation of the amorphous MoO_x layer need to be further analyzed in the future. It could be demonstrated that patterning of an MoS_2 bilayer down to a monolayer at selected positions is possible applying laser-thinning. The results indicate a huge potential for high-degree controlled 2D monolayer fabrication.

For MoS_2 and other semiconducting TMDCs, PL monitoring during laser-thinning is more suitable compared to Raman monitoring. The clear shift or vanishing of the indirect band gap and a strong increase of the A exciton PL intensity are strong indicators for a change of the number of layers. PL monitoring has the potential to significantly increase the process speed and precision of laser-thinning as the PL intensity typically is one order

of magnitude higher compared to the respective Raman signals. However, in case of laser-thinning of heterostructures consisting of semi- or superconducting TMDCs, insulators such as BN and semimetals such as graphene, PL monitoring alone would not be sufficient. For optically inactive materials, Raman monitoring is required. It is expected that the laser-thinning method can also be applied to other 2D semiconductors such as WS_2, $MoSe_2$ and WSe_2.

Methods

Exfoliation. Exfoliation of MoS_2 bulk crystals is performed by repeatedly peeling off MoS_2 sheets between two adhesive gel films and finally pressing the film onto a SiO_x/Si wafer which leads to randomly distributed flakes of mono- and multilayers on the substrate. The thickness of the SiO_x layer obtained by dry thermal oxidation amounting to 285 nm enhances the visiblity of the thin layers through the optical microscope.[42]

Raman and PL Spectroscopy, Laser-Thinning. Raman and PL spectra were recorded using a customized Horiba LabRAM HR Evolution at room temperature under ambient conditions. Raman measurements were performed using a 325 nm HeCd laser in continuous wave (cw) operation for excitation. The laser was focussed by use of a 40× mirror objective with a numerical aperture (NA) of 0.5 to a spot size of $\sim 1\,\mu m$. PL measurements were carried out utilizing a 406 nm laser diode in cw operation. The laser spot size was $\sim 0.5\,\mu m$ using a 100× objective with an NA of 0.9. The laser power on the sample was set to 5 mW for Raman and PL measurements during laser-thinning. For characterization without laser-thinning, the laser power was reduced by a factor of 4 for both Raman and PL identification and mapping.

XPS measurements. The XPS measurements were performed using a Thermo K-Alpha System equipped with a monochromatized Al K_α X-ray source (1468.6 eV). The specimen was localized by focusing the X-ray spot to enable a lateral resolution of around 50 µm and

image the Mo 3d signal using the snapshot mode at a pass energy of 150 eV. Survey and high resolution spectra were acquired at pass energies of 150 and 20 eV, respectively. The energy scale was referenced to the binding energy of adventitious carbon of 248.8 eV as an internal reference. The spectral analysis was performed by using CasaXPS (v2.3.19) and GL(30) lineshapes.

AFM measurements. Surface topography was measured with a Bruker Dimension Icon3 and a Nanoscope V SPM control unit using a proprietary off-resonant intermittent contact mode (PeakForce QNM mode) and Pt-coated cantilevers (8 N/m, HQ:XSC11/Pt, MikroMasch).

Author Information

Corresponding author

E-mail: tessarek@ifp.uni-bremen.de

ORCID

Christian Tessarek: 0000-0003-4126-3694

Martin Eickhoff: 0000-0001-6493-269X

Notes

The authors declare no competing financial interest.

Acknowledgement

The research leading to these results has received funding from the Central Research Development Fund (CRDF) of the University of Bremen. O.G. thanks the German Academic Exchange Service (DAAD) for support. The authors thank Philip Klement from the Justus-Liebig University of Giessen, Germany, for providing an introduction into sample preparation.

References

(1) Li, T.; Galli, G. Electronic Properties of MoS_2 Nanoparticles. *J. Phys. Chem. C* **2007**, *111*, 16192.

(2) Lebègue, S.; Eriksson, O. Electronic structure of two-dimensional crystals from ab initio theory. *Phys. Rev. B* **2009**, *79*, 115409.

(3) Splendiani, A.; Sun, L.; Zhang, Y.; Li, T.; Kim, J.; Chim, C.-Y.; Galli, G.; Wang, F. Emerging Photoluminescence in Monolayer MoS_2. *Nano Lett.* **2010**, *10*, 1271.

(4) Mak, K. F.; Lee, C.; Hone, J.; Shan, J.; Heinz, T. F. Atomically Thin MoS_2: A New Direct-Gap Semiconductor. *Phys. Rev Lett.* **2010**, *105*, 136805.

(5) Mishra, H.; Bose, A.; Dhar, A.; Bhattacharya, S. Exciton-phonon coupling and band-gap renormalization in monolayer WSe_2. *Phys. Rev. B* **2018**, *98*, 045143.

(6) Lee, Y.-H.; Zhang, X.-Q.; Zhang, W.; Chang, M.-T.; Lin, C.-T.; Chang, K.-D.; Yu, Y.-C.; Wang, J. T.-W.; Chang, C.-S.; Li, L.-J.; Lin, T.-W. Synthesis of Large-Area MoS_2 Atomic Layers with Chemical Vapor Deposition. *Adv. Mater.* **2012**, *24*, 2320.

(7) Hall, J.; Pielić, B.; Murray, C.; Jolie, W.; Wekking, T.; Busse, C.; Kralj, M.; Michely, T. Molecular beam epitaxy of quasi-freestanding transition metal disulphide monolayers on van der Waals substrates: a growth study. *2D Mater.* **2018**, *5*, 025005.

(8) Eda, G.; Yamaguchi, H.; Voiry, D.; Fujita, T.; Chen, M.; Chhowalla, M. Photoluminescence from Chemically Exfoliated MoS_2. *Nano Lett.* **2011**, *11*, 5111.

(9) Li, H.; Wu, J.; Yin, Z.; Zhang, H. Preparation and Applications of Mechanically Exfoliated Single-Layer and Multilayer MoS_2 and WSe_2 Nanosheets. *Acc. Chem. Res.* **2014**, *47*, 1067.

(10) Li, X.; Tao, L.; Chen, Z.; Fang, H.; Li, X.; Wang, X.; Xu, J.-B.; Zhu, H. Graphene and related two-dimensional materials: Structure-property and relationships for electronics and optoelectronics. *Appl. Phys. Rev.* **2017**, *4*, 021306.

(11) Qin, C.; Gao, Y.; Qiao, Z.; Xiao, L.; Jia, S. Atomic-Layered MoS_2 as a Tunable Optical Platform. *Adv. Optical Mater.* **2016**, *4*, 1429.

(12) Venkatakrishnan, A.; Chua, H.; Tan, P.; Hu, Z.; Liu, H.; Liu, Y.; Carvalho, A.; Lu, J.; Sow, C. H. Microsteganography on WS_2 Monolayers Tailored by Direct Laser Painting. *ACS Nano* **2017**, *11*, 713.

(13) Castellanos-Gomez, A.; Barkelid, M.; Goossens, A. M.; Calado, V. E.; van der Zant, H. S. J.; Steele, G. A. Laser-Thinning of MoS_2: On Demand Generation of a Single-Layer Semiconductor. *Nano Lett.* **2012**, *12*, 3187.

(14) Lu, J.; Lu, J. H.; Liu, H.; Liu, B.; Chan, K. X.; Lin, J.; Chen, W.; Loh, K. P.; Sow, C. H. Improved Photoelectrical Properties of MoS_2 Films after Laser Micromachining. *ACS Nano* **2014**, *8*, 6334.

(15) Gu, E.; Wang, Q.; Zhang, Y.; Cong, C.; Hu, L.; Tian, P.; Liu, R.; S.-L-Zhang,; Qiu, Z.-J. A real-time Raman spectroscopy study of the dynamics of laser-thinning of MoS_2 flakes to monolayers. *AIP Advances* **2017**, *7*, 125329.

(16) Hu, L.; Shan, X.; Wu, Y.; Zhao, J.; Lu, X. Laser Thinning and Patterning of MoS_2 with Layer-by-Layer Precision. *Sci. Rep.* **2017**, *7*, 15538.

(17) Gong, L.; Zhang, Q.; Wang, L.; Wu, J.; Han, C.; Lei, B.; Chen, W.; Eda, G.; Goh, K. E. J.; Sow, C. H. Emergence of photoluminescence on bulk MoS_2 by laser thinning and gold particle decoration. *Nano Res.* **2018**, *11*, 4574.

(18) Mine, H.; Kobayashi, A.; Nakamura, T.; Inoue, T.; Pakdel, S.; Marian, D.; Gonzalez-Marin, E.; Maruyama, S.; Katsumoto, S.; Fotrunelli, A.; Palacios, J. J.; Haruyama, J.

Laser-Beam-Patterned Topological Insulating States on Thin Semiconducting MoS_2. *Phys. Rev. Lett.* **2019**, *123*, 146803.

(19) Rho, Y.; Pei, J.; Wang, L.; Su, Z.; Eliceiri, M.; Grigoropoulos, C. P. Site-Selective Atomic Layer Precision Thinning of MoS_2 via Laser-Assisted Anisotropic Chemical Etching. *ACS Appl. Mater. Interfaces* **2019**, *11*, 39385.

(20) Tran-Khac, B.-C.; White, R. M.; DelRio, F. W.; Chung, K. Layer-by-layer thinning of MoS_2 via laser irradiation. *Nanotechnology* **2019**, *30*, 275302.

(21) Lee, C.; adn L. E. Brus, H. Y.; Heinz, T. F.; Hone, J.; Ryu, S. Anomalous Lattice Vibrations of Single- and Few-Layer MoS_2. *ACS Nano* **2010**, *4*, 2695.

(22) Castellanos-Gomez, A.; van der Zant, H. S. J.; Steele, G. A. Folded MoS_2 layers with reduced interlayer coupling. *Nano Res.* **2014**, *7*, 572.

(23) Placidi, M.; Dimitrievska, M.; Izquierdo-Roca, V.; Fontané, X.; Castellanos-Gomez, A.; Pérez-Tomás, A.; Mestres, N.; Espindola-Rodriguez, M.; López-Marino, S.; Neuschitzer, M.; Bermudez, V.; Yaremko, A.; Pérez-Rodríguez, A. Multiwavelength excitation Raman scattering analysis of bulk and two-dimensional MoS_2: vibrational properties of atomically thin MoS_2 layers. *2D Mater.* **2015**, *2*, 035006.

(24) Sun, L.; Yan, J.; Zhan, D.; Liu, L.; Hu, H.; Li, H.; Tay, B. K.; Kuo, J.-L.; Huang, C.-C.; Hewak, D. W.; Lee, P. S.; Shen, Z. X. Spin-Orbit Splitting in Single-Layer MoS_2 Revealed by Triply Resonant Raman Scattering. *Phys. Rev. Lett.* **2013**, *111*, 126801.

(25) Lee, J.-U.; Park, J.; Son, Y.-W.; Cheong, H. Anomalous excitonic resonance Raman effects in few-layered MoS_2. *Nanoscale* **2015**, *7*, 3229.

(26) Ross, J. S.; Wu, S.; Yu, H.; Ghimire, N. J.; Jones, A. M.; Aivazian, G.; Yan, J.; Mandrus, D. G.; Xiao, D.; Yao, W.; Xu, X. Electrical control of neutral and charged excitons in a monolayer semiconductor. *Nat. Commun.* **2012**, *3*, 887.

(27) Berkelbach, T. C.; Hybertsen, M. S.; Reichmann, D. R. Theory of neutral and charged excitons in monolayer transition metal dichalcogenides. *Phys. Rev. B* **2013**, *88*, 045318.

(28) Tongay, S.; Zhou, J.; Ataca, C.; Liu, J.; Kang, J. S.; Matthews, T. S.; You, L.; Li, J.; Grossmann, J. C.; Wu, J. Broad-Range Modulation of Light Emission in Two-Dimensional Semiconductors by Molecular Physisorption Gating. *Nano Lett.* **2013**, *13*, 2831.

(29) Zahid, F.; Liu, L.; Zhu, Y.; Wang, J.; Guo, H. A generic tight-binding model for monolayer, bilayer and bulk MoS_2. *AIP Adv.* **2013**, *3*, 052111.

(30) Kuc, A.; Zibouche, N.; Heine, T. Influence of quantum confinement on the electronic structure of the transition metal sulfide TS_2. *Phys. Rev. B* **2011**, *83*, 245213.

(31) Ajito, K.; Nagahara, L. A.; Tryk, D. A.; Hashimoto, K.; Fujishima, A. Study of Photochromic Properties of Amorphous MoO_3 Films Using Raman Microscopy. *J. Phys. Chem.* **1995**, *99*, 16383.

(32) Alrasheed, A.; Gorham, J. M.; Khac, B. C. T.; Alsaffar, F.; DelRio, F. W.; Chung, K.-H.; Amer, M. R. Surface Properties of Laser-Treated Molybdenum Disulfide Nanosheets for Optoelectronic Applications. *ACS Appl. Mater. Interfaces* **2018**, *10*, 18104.

(33) Liang, L.; Meunier, V. First-principles Raman spectra of MoS_2, WS_2 and their heterostructures. *Nanoscale* **2014**, *6*, 5394.

(34) Horynová, E.; Romanyuk, O.; Horák, L.; Remeš, Z.; Conrad, B.; Amalathas, A. P.; Landová, L.; Houdková, J.; Jiříček, P.; Finsterle, T.; Holovský, J. Optical characterization of low temperature amorphous MoO_x, WO_x, and VO_x prepared by pulsed laser deposition. *Thin Sol. Films* **2020**, *693*, 137690.

(35) The total time for a single PL measurement from 500 nm to 1050 nm is 10× longer compared to the integration time of a single Raman spectrum due to the moving grating

of the spectrometer (spectral window of single acquisition was 55 nm, aquisition time per spectral window was 1 s).

(36) Wu, K.; Li, Z.; Tang, J.; Lv, X.; Wang, H.; Luo, R.; Liu, P.; Qian, L.; Zhang, S.; Yuan, S. Controllable defects implantation in MoS_2 grown by chemical vapor deposition for photoluminescence enhancement. *Nano Res.* **2018**, *11*, 4123.

(37) Oh, H. M.; Han, G. H.; Kim, H.; Bae, J. J.; Jeong, M. S.; Lee, Y. H. Photochemical Reaction in Monolayer MoS_2 via Correlated Photoluminescence, Raman Spectroscopy, and Atomic Force Microscopy. *ACS Nano* **2016**, *10*, 5230.

(38) Klement, P.; Steinke, C.; Chatterjee, S.; Wehling, T. O.; Eickhoff, M. Effects of the Fermi level energy on the adsorption of O_2 to monolayer MoS_2. *2D Mater.* **2018**, *5*, 045025.

(39) Nan, H.; Wang, Z.; Hang, W.; Liang, Z.; Lu, Y.; Chen, Q.; He, D.; Tan, P.; Miao, F.; Wang, X.; Wang, J.; Ni, Z. Strong Photoluminescence Enhancement of MoS_2 through Defect Engineering and Oxygen Bonding. *ACS Nano* **2014**, *8*, 5738.

(40) Han, G. H.; Chae, S. J.; Kim, E. S.; Günes, F.; Lee, I. H.; Lee, S. W.; Lee, S. Y.; Lim, S. C.; Jeong, H. K.; Jeong, M. S.; Lee, Y. H. Laser Thinning for Monolayer Graphene Formation: Heat Sink and Interference Effect. *ACS Nano* **2011**, *5*, 263.

(41) Cui, X.-Y.; Ringer, S. P.; Wang, G.; Stachurski, Z. H. What should the density of amorphous solids be? *J. Chem. Phys.* **2019**, *151*, 194506.

(42) Benameur, M. M.; Radisavljevic, B.; Héron, J. S.; Sahoo, S.; Berger, H.; Kis, A. Visibility of dichalcogenide nanolayers. *Nanotechnology* **2011**, *22*, 125706.